Ocean Engineering 36 (2009) 113–118

Contents lists available at ScienceDirect

Ocean Engineering

journal homepage: www.elsevier.com/locate/oceaneng

Experimental investigation of hydrodynamic force coefficients over AUV hull form

P. Jagadeesh [a,*], K. Murali [b], V.G. Idichandy [b]

[a] School of Mechanical Engineering, The University of Western Australia, 35 Stirling Highway, Perth, WA 6009, Australia
[b] Department of Ocean Engineering, Indian Institute of Technology Madras, Chennai, India

ARTICLE INFO

Article history:
Received 24 June 2008
Accepted 13 November 2008
Available online 7 December 2008

Keywords:
Autonomous underwater vehicles
Axisymmetric underwater body
CFD
Hydrodynamic force coefficients
Towing tank measurements

ABSTRACT

Extensive use of autonomous underwater vehicles (AUVs) in oceanographic applications necessitates investigation into the hydrodynamic forces acting over an AUV hull form operating under deeply submerged condition. This paper presents a towing tank-based experimental study on forces and moment on AUV hull form in the vertical plane. The AUV hull form considered in the present program is a 1:2 model of the standard hull form Afterbody1. The present measurements were carried out at typical speeds of autonomous underwater vehicles (0.4–1.4 m/s) by varying pitch angles (0–15°). The hydrodynamic forces and moment are measured by an internally mounted multi-component strain gauge type balance. The measurements were used to study variation of axial, normal, drag, lift and pitching moment coefficients with Reynolds number (Re) and angle of attack. The measurements have also been used to validate results obtained from a CFD code that uses Reynolds Average Navier–Stokes equations (ANSYS^{TM} Fluent). The axial and normal force coefficients are increased by 18% and 195%; drag, lift and pitching moment coefficients are increased by 90%, 182% and 297% on AUV hull form at $\alpha = 15^{\circ}$ and $Re_v = 3.65 \times 10^5$. These results can give better idea for the efficient design of guidance and control systems for AUV.

1. Introduction

In view of increasing the importance of deep ocean resources, application of underwater vehicle (UWV) is extended to a wide range of areas such as exploration and exploitation of seafloor minerals, environmental monitoring and protection and deep sea exploration of hydrocarbons up to 6000 m. This emphasizes the need for better understanding of the hydrodynamic forces acting on the underwater bodies under various conditions. Such understanding will lead to more efficient powering systems for the UWV. The present investigation sets out to address this aspect, there by aiming to investigate the hydrodynamic force coefficients—drag, lift and pitching moment coefficients acting over a typical underwater body at various angles of attack and speed. While measurements provide valuable data, most of the experimental investigations on axisymmetric underwater bodies have been conducted in a wind tunnel (Gertler, 1950; Granville, 1953; Nakayama and Patel, 1974; Patel and Lee, 1977; Huang et al., 1978; Roddy, 1990; Anil Dash et al., 1996; Hackett, 2000). Zedan and Dalton (1979) made a critical comparison between the drag characteristics based on volume, surface area and frontal area for different axisymmetric bodies. Sayer (1996) measured drag and added mass coefficients on a ROV and a solid box for various depths of submergence from the free surface in a towing tank. However, hydrodynamic coefficients derived from the towing tank experimental investigations are limited in literature. Recently, this is overcome by applying computational fluid dynamics (CFD) techniques. Several authors (Patel and Chen, 1986; Choi and Ching, 1991; Sung et al., 1993, 1995; Sarkar et al., 1997a, b; Ananthakrishnan and Zhang, 1998; Mulvany et al., 2004; Jagadeesh and Murali, 2006) investigated various issues related to the application of CFD to underwater hydrodynamics. Selection of turbulence models, grid generation and boundary resolution techniques, influence of boundary conditions on CFD solutions, etc. were investigated over axisymmetric bodies. The review of literature also revealed that Reynolds number (Re) for practical applications existed in the transition regime ($1 \times 10^5 < Re = \rho UL/\mu < 1 \times 10^6$) and hence there is a need for low-Re k-ε turbulence models and related knowledge. The low-Re models are expected to give better results as they are superior in prediction of entire boundary layer over underwater hull form. Therefore, finding a suitable turbulence model for three-dimensional (3D) simulation of hydrodynamic characteristics on Afterbody1 for autonomous underwater vehicle (AUV) operating conditions will

* Corresponding author. Tel.: +61 8 64888151; fax: 61 8 64881024.
E-mail addresses: jputta@mech.uwa.edu.au, jagadeeshiitm@yahoo.com (P. Jagadeesh).

0029-8018/$ - see front matter © 2008 Elsevier Ltd. All rights reserved.
doi:10.1016/j.oceaneng.2008.11.008

have paramount importance for the future hydrodynamic investigations at practical conditions.

Hence, in the current investigations forces on conducting towing tank experimental studies on *Afterbody1* to determine hydrodynamic characteristics for AUV operating speeds, ranging from 0.4 m/s ($Re_v = 1.05 \times 10^5$) to 1.4 m/s ($Re_v = 3.67 \times 10^5$) for different angles of attack. Following a two pronged approach, numerical studies are conducted using low-*Re* k-ε turbulence model for reproducing the experimentally measured quantities in CFD. The CFD investigations have been carried out by implementing the low-*Re* models in the commercial flow solver FLUENT. The measured and computed forces coefficients are compared in the range of $Re_v = \rho U \nabla^{1/3}/\mu$ (1.05×10^5–3.67×10^5) for various angles of attack (α). The angles of attack considered are 0°, 5°, 10° and 15°. The studies suggest that the force coefficients very significantly as a function of angle of attack, α. On the otherhand, the CFD procedure is shown to be capable of reproducing the experimental investigations quite well.

2. Experimental programme

2.1. Experimental setup

The AUV hull form considered for the current investigation is Afterbody1 by Huang et al. (1978). The length to diameter (L/D) ratio for Afterbody1 is 10.9745. A model scale ratio of 1:2 was selected for the experimental body using Froude scaling. The total length and maximum diameter of the model was 1.4 and 0.14 m ($L/D = 10.0$), respectively. The tail portion of the model was slightly adjusted in order to accommodate sting/L-frame for a captive towing test along with force balance arrangement given in Fig. 1. Model was fabricated out of aluminium and was anodized to prevent it from abrasion during towing in submerged condition. The interior of the model was not allowed to flood during submerged condition. An L-frame was fabricated using seamless steel pipe with adequate stiffness. The exact depth of submergence of the model from the free surface was maintained by the marking depth of submergence, $d = 4.0$, 6.0, 0.8 and 10.0D (where D is the maximum diameter of the model) on the vertical arm of the L-Frame. Experimental parameters and their range considered in the current investigation are given in Table 1. The towing carriage was fitted with tachometer as well as digital monitor, distance-timer to measure the carriage speed.

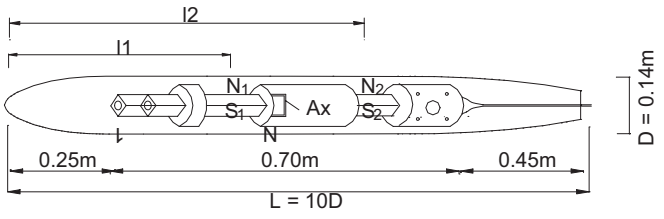

Fig. 1. Experimental model with force balance and strain gauge locations.

Table 1
Parameters considered in captive towing tests.

Parameters	Units	Description
Velocity	m/s	0.4, 0.6, 0.8, 1.0, 1.2 and 1.4
Relative submergence depth (d/D)	–	4.0, 6.0, 8.0 and 10.0
Reynolds number ($\times 10^5$)	–	1.05, 1.57, 2.10, 2.62, 3.15 and 3.67
Angle of attack (α)	deg.	0, 5, 10 and 15
Hydrodynamic coefficients	–	Drag, lift and pitching moment

A five component force balance was used for measuring the hydrodynamic forces acting on model AUV hull form. The force balance was capable of measuring axial, normal and side forces and moments in pitching and yawing simultaneously. It has been fabricated in-house by Anil Dash et al. (1996). Force balance has been calibrated frequently in order to check for linearity and calibration constants through out the period of experimentation. The resultant force (N) on the sensors can be obtained using these calibration constants as follows,

$$\text{Force } (N) = a_x(\text{volts}) \times \text{calibration constant(kg/volts)} \times 9.81\,(\text{m/s}^2) \quad (1)$$

where a_x is the typical output corresponding to axial load from axial sensor. Similarly, for each of the other loading conditions (N_1, N_2, S_1 and S_2) the calibration is obtained. The loads on each sensor [O] and the resultant forces in each direction [f] are linked by the calibration matrix [R] as given below

$$[R][f] = [O] \quad (2)$$

where [R] is the calibration matrix; [f] is the force matrix; [O] is the output (sensor-based force) matrix.

The calibration matrix was formed by filling the elements of a matrix by values from corresponding calibration curves which is obtained as

$$\begin{bmatrix} 0.2464 & -0.0057 & -0.0002 & 0.0070 & 0.0035 \\ 0.0075 & 0.2634 & -0.0071 & -0.0009 & 0.0074 \\ -0.0006 & 0.2350 & 0.2477 & -0.0043 & 0.0027 \\ -0.0161 & -0.0003 & 0.0078 & 0.2637 & 0.0045 \\ -0.0056 & 0.0106 & -0.0154 & -0.0226 & 0.3127 \end{bmatrix} \begin{bmatrix} N_1 \\ N_2 \\ S_1 \\ S_2 \\ Ax \end{bmatrix} = \begin{bmatrix} n_1 \\ n_2 \\ s_1 \\ s_2 \\ a_x \end{bmatrix} \quad (3)$$

where N_1, N_2 and S_1, S_2 and Ax are strain gauges measuring normal force, side force and axial forces, respectively. And n_1, n_2 and s_1, s_2 and a_x are total normal force, side force and axial force acting on the AUV hull form. Microsoft Windows based software package, HP Benchlink Data logger was used with a PC for data acquisition.

2.2. Experimental procedure

A schematic representation of the experimental setup is shown in Fig. 2. Series of tests were conducted in a towing tank for the

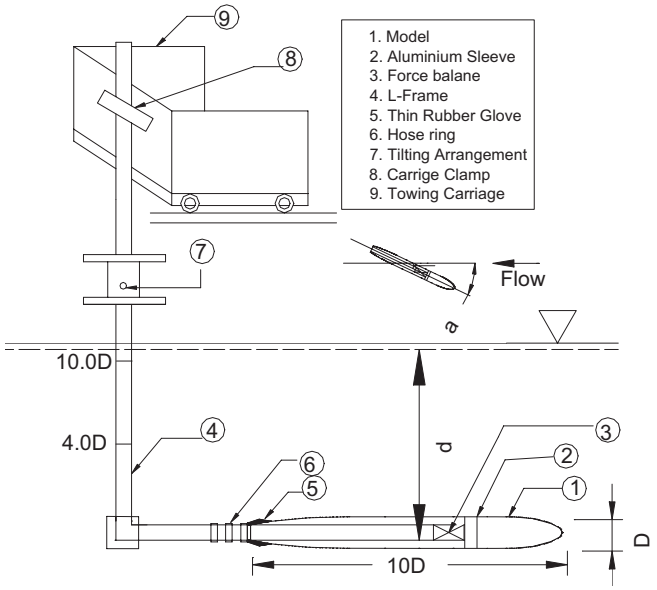

Fig. 2. Experimental setup in the towing tank.

range of experimental variables, as mentioned earlier. The hydrodynamic coefficients does not show much change for $d/D = 4.0$, 6.0, 8.0 and 10.0, only one set of results are presented encompassing different speeds and angles of attack. Data collection time for each run consists of stationary, accelerating and steady, and decelerating phases of the carriage. Resultant forces [f] were obtained solving the matrix Eq. (5). The $[R]^{-1}$ obtained for this purpose is given below.

$$[f][R]^{-1}[O] \tag{4}$$

$$\{f\} = \begin{Bmatrix} N_1 \\ N_2 \\ S_1 \\ S_2 \\ Ax \end{Bmatrix} = \begin{bmatrix} 4.0475 & 0.0888 & 0.0064 & -0.1110 & -0.0459 \\ -0.1164 & 3.7884 & 0.1026 & 0.1026 & -0.0893 \\ 0.0241 & -0.3573 & 4.0232 & 0.0614 & -0.0274 \\ 0.2448 & 0.0189 & 0.0189 & -0.1218 & -0.0565 \\ 0.0953 & -0.1431 & 0.1860 & 0.2738 & 3.1947 \end{bmatrix} \times \begin{Bmatrix} n_1 \\ n_2 \\ s_1 \\ s_2 \\ a_x \end{Bmatrix} \tag{5}$$

The final forces and moments acting on the model in the body coordinate system are obtained as follows:

$$\text{Axial force}(F_A) = Ax \tag{6}$$

$$\text{Normal force}(F_N) = N_1 + N_2 \tag{7}$$

$$\text{Pitching moment}(M_Z) = N_1 l_1 - N_2 l_2 \tag{8}$$

where suffix l_1 and l_2 represent the strain gauge location from nose of the model. It may be noted that the side forces S1 and S2 are discarded.

The axial and normal force coefficients are obtained as follows:

$$C_A = F_A/(0.5\rho U^2 \nabla^{2/3}) \tag{9}$$

$$C_N = F_N/(0.5\rho U^2 \nabla^{2/3}) \tag{10}$$

To maintain uniformity in presentation of the force components both in experimental and numerical investigations, it is essential to resolve measured forces from body coordinate system to tank fixed coordinate system, as shown in Fig. 3. Hence, the data from each run was used to obtain the drag and lift forces on the body by resolving the axial and normal component of the forces from the body coordinate system to the tank fixed coordinate system as follows:

$$\text{Drag force}(F_D) = F_A \cos\alpha^\circ - F_N \sin\alpha^\circ\theta \tag{11}$$

$$\text{Lift force}(F_L) = -(F_N \cos\alpha^\circ + F_A \sin\alpha^\circ) \tag{12}$$

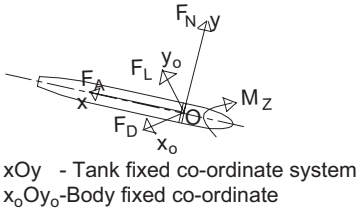

Fig. 3. Body and tank fixed co-ordinate systems and component forces.

The drag, lift and pitching moment coefficients are obtained as follows:

$$C_{DV} = F_D/(0.5\rho U^2 \nabla^{2/3}) \tag{13}$$

$$C_{LV} = F_L/(0.5\rho U^2 \nabla^{2/3}) \tag{14}$$

$$C_{MV} = M_z/(0.5\rho U^2 \nabla^{2/3} L) \tag{15}$$

where in C_{DV} is drag force coefficient, C_{LV} is lift force coefficient, C_{MV} is pitching moment (about nose) coefficient, ρ is the density of water, U is the towing speed, ∇ is volume of the body, L is length of the body and α is angle of attack in degrees. The maximum overall uncertainty in the measured values was estimated to be of the order of 6.25% and 6.82% for drag and lift coefficients. The same is about 7% for pitching moment coefficient.

3. Numerical modelling

Authors selected k-ε AKN (Abe et al., 1994) turbulence model for numerical investigation based on their previous experience in two-dimensional (2D)-axisymmetric studies for similar type of bodies (Jagadeesh and Murali, 2005, 2006) in order to validate application of low-*Re* turbulence models for 3D underwater hydrodynamic applications.

3.1. Governing equations

The general form of the continuity and Navier–Stokes equations with Reynolds averaging (Wilcox and Rubesin, 1980) are used along with the k-ε model equation as explained below

$$\frac{\partial k}{\partial t} + U_j \frac{\partial k}{\partial x_j} = \nu_t \left(\frac{\partial U_i}{\partial x_j} + \frac{\partial U_j}{\partial x_i}\right)\frac{\partial U_i}{\partial x_j} - \varepsilon + \frac{\partial}{\partial x_j}\left[(\nu + \nu_t/\sigma_k)\frac{\partial k}{\partial x_f}\right] + D \tag{16}$$

$$\frac{\partial \varepsilon}{\partial t} + U_j \frac{\partial \varepsilon}{\partial x_j} = f_1 C_{\varepsilon 1} \frac{\varepsilon}{k} \nu_t \left(\frac{\partial U_i}{\partial x_j} + \frac{\partial U_j}{\partial x_i}\right)\frac{\partial U_i}{\partial x_j} - f_2 C_{\varepsilon 2} \frac{\varepsilon^2}{k} + \frac{\partial}{\partial x_j}\left[(\nu + \nu_t/\sigma_k)\frac{\partial k}{\partial x_f}\right] + E \tag{17}$$

$$\nu_t = f_\mu C_\mu \frac{k^2}{\varepsilon} \tag{18}$$

where U_i is the mean velocity vector of the flow, ν_t is turbulent kinematic viscosity, f_μ is damping function, C_μ is model constant, k is turbulent kinetic energy and ε is energy dissipation rate.

In comparison of the standard closure models, the low-*Re* k-ε equations contain damping functions f_μ, f_1 and f_2, destruction terms D and E, and molecular diffusion terms. And also the values of model constants, C_μ, $C_{\varepsilon 1}$ and $C_{\varepsilon 2}$ are to be specified by the user and are different for different models. Model constants for k-ε AKN model are: $C_\mu = 0.09$, $C_{\varepsilon 1} = 1.50$, $C_{\varepsilon 2} = 1.90$, $\sigma_k = 1.40$ and $\sigma_\varepsilon = 1.40$. In addition to that of the terms $D = 0$ and $E = 0$. The damping functions considered in this model are

$$f_\mu = \left[1 - \exp\left(\frac{-y^k}{14}\right)\right]^2 \left[1 + \frac{5}{R_T^{3/4}} \exp\left\{-\left(\frac{R_T}{200}\right)^2\right\}\right]; \quad f_{\varepsilon 1} = 1;$$

$$f_{\varepsilon 2} = \left[1 - \exp\left(\frac{-y^k}{3.1}\right)\right]^2 \left[1 - 0.3\left\{-\left(\frac{R_T}{6.5}\right)^2\right\}\right]$$

where $y^k = u_\varepsilon y/\nu$ and $R_y = y k^{1/2}/\nu$.

For more details on low-*Re* turbulence models, model constants and notations readers are advised to refer ANSYS™ Fluent manual.

3.2. Boundary conditions

The boundary conditions considered at various boundaries are, for inlet-velocity inlet with velocity that varies from 0.4 to 1.4 m/s with an increment of 0.2 m/s, for outlet-outflow condition, for hull-wall with no slip condition and farfield-wall with no slip (zero specified shear) and over body surface $k = 0$; $\varepsilon = 2\nu(\partial\sqrt{k}/\partial y)^2$.

3.3. Modelling and grid independence analysis

A solution domain of size 39DX10DX5D (where D = maximum diameter of the body) had arrived based on domain independence study carried for each domain ($46D \times 12D \times 6D$; $39D \times 10D \times 5D$; $31D \times 10D \times 4D$; $25D \times 10D \times 3D$), was processed using k-ε AKN turbulence model at a free stream velocity of 1.4 m/s for zero angle of attack. The computational domain was extended 7D in front of the leading edge of the underwater hull form, 26D behind the trailing edge, 5D above and below the hull surface and 5D normal to x–y plane (z-direction). To obtain accurate estimation of hydrodynamic coefficients, the solution domain was discretized into quadrilateral cells resulting in a structure grid. For grid independence study, solution domain was tested with grid densities of 0.23, 0.33, 0.46 and 0.65 million cells, respectively, using k-ε AKN turbulence. It was inferred from the grid independence study, solution have been converged for 0.46 million cells, which corresponds to a cell Reynolds number, $Re_{(\mathrm{cell})} = \rho u l/\mu = 3.02 \times 10^3$, where '$l$' is the minimum length of the cell on the model. The convergence criteria adopted in this study of the order of 10^{-4}, for all the solution residues.

4. Results and discussion

4.1. Stud effect on measurements

The influence of stud on hydrodynamic force coefficients is assessed by the numerical estimation of stud effect on drag coefficient. Numerical studies are performed with and without stud on Afterbody1 at $\alpha = 0^\circ$ corresponding to a maximum speed of 1.4 m/s ($Re_v = 3.67 \times 10^5$). Results from numerical studies are revealed that the drag coefficient is over predicted by 2% with stud when compared to a no stud condition. Henceforth, the pressure correction at tail end of the model due to stud is not considered in the current investigation due to its insignificant small value.

4.2. Influence of Reynolds number on axial and normal force coefficients

Measured axial force coefficient (C_A) and its variation with Re_v at various angles of attack are presented in Fig. 4. It is observed that the C_A value decreases by 21%, 18%, 17% and 16%, for $\alpha = 0^\circ$, 5°, 10° and 15° in the range of Re_v, 1.05×10^5–3.67×10^5. This may be attributed to the fact that as velocity increases the pressure decreases without significant change in frictional resistance. Therefore, C_A value decreases with increase in Re_v. And also observed an overall increase in C_A value by 8%, 12% and 18% as 'α' increases from 0° to 5°, 10° and 15° with respect to $\alpha = 0^\circ$ and $Re_v = 3.67 \times 10^5$. Reason for this behaviour of C_A is the increase of pressure force with increases in angle of attack resembling the blockage effect. So, the reduction of axial force coefficient is less with increase in Re_v at higher angles of attack.

Fig. 5 shows the variation of normal force coefficient (C_N) with Re_v for $\alpha = 5^\circ$, 10° and 15°. The value of C_N decreases by 9%, 9% and 11% for $\alpha = 5^\circ$, 10° and 15° in the range of Reynolds number

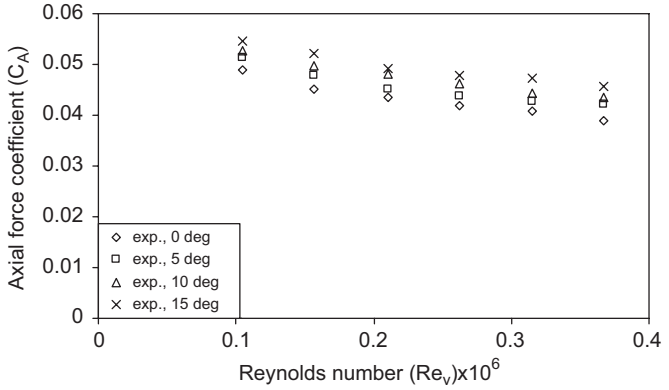

Fig. 4. Influence of Reynolds number (Re_v) on axial force coefficient for various angles of attack.

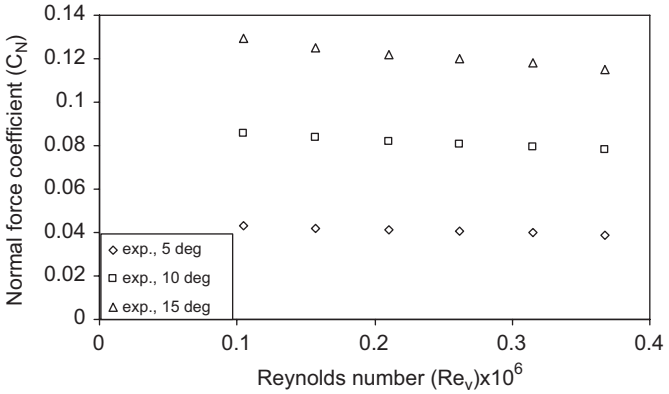

Fig. 5. Influence of Reynolds number (Re_v) on normal force coefficient for various angles of attack.

considered. As the angle of attack increases from $\alpha = 5^\circ$ to 10° and 15°, the C_N value increase by 100% and 195%, for $Re_v = 3.67 \times 10^5$. The main source for huge increase in C_N value at higher angles of attack is the flow separation point shifts from aft body (tail) to nose (fore body) and it creates negative pressure over the bottom surface of the body. Hence, the uplift force acting on the body coupled with excess force generated due to negative pressure increases overall normal force acting on the body.

4.3. Effect of Reynolds number on C_{DV}, C_{LV} and C_{MV}—A comparison between measured and numerical results

Fig. 6 depicts the variation of C_{DV}, C_{LV} and C_{MV} with Re_v for various angles of attack and also comparison between measured and numerical results. It is observed from figure, the C_{DV} value decreases by 26%, 21%, 18% and 17% for $\alpha = 0^\circ$, 5°, 10° and 15° in the range of Re_v from 1.05×10^5 to 3.67×10^5. And its value increases by 17%, 45% and 90% as α increases from 0° to 5°, 10° and 15° with reference to $\alpha = 0^\circ$ and $Re_v = 3.67 \times 10^5$. Similar to C_A, the drag coefficient value also decreases with increase in Re_v at higher angles of attack. The above distinctive feature of C_{DV} can be explained from numerical studies carried out for the test conditions using k-ε AKN turbulence model. The main reason for this behaviour of C_{DV} is, as the angle of attack increases the pressure drag coefficient increases, but there is only a marginal change in friction (skin friction) coefficient. Also, at higher angles of attack the reduction of pressure drag coefficient decreases with increase in Re_v. Table 2 shows typical CFD results of pressure, friction and total drag coefficient values for Afterbody1 at

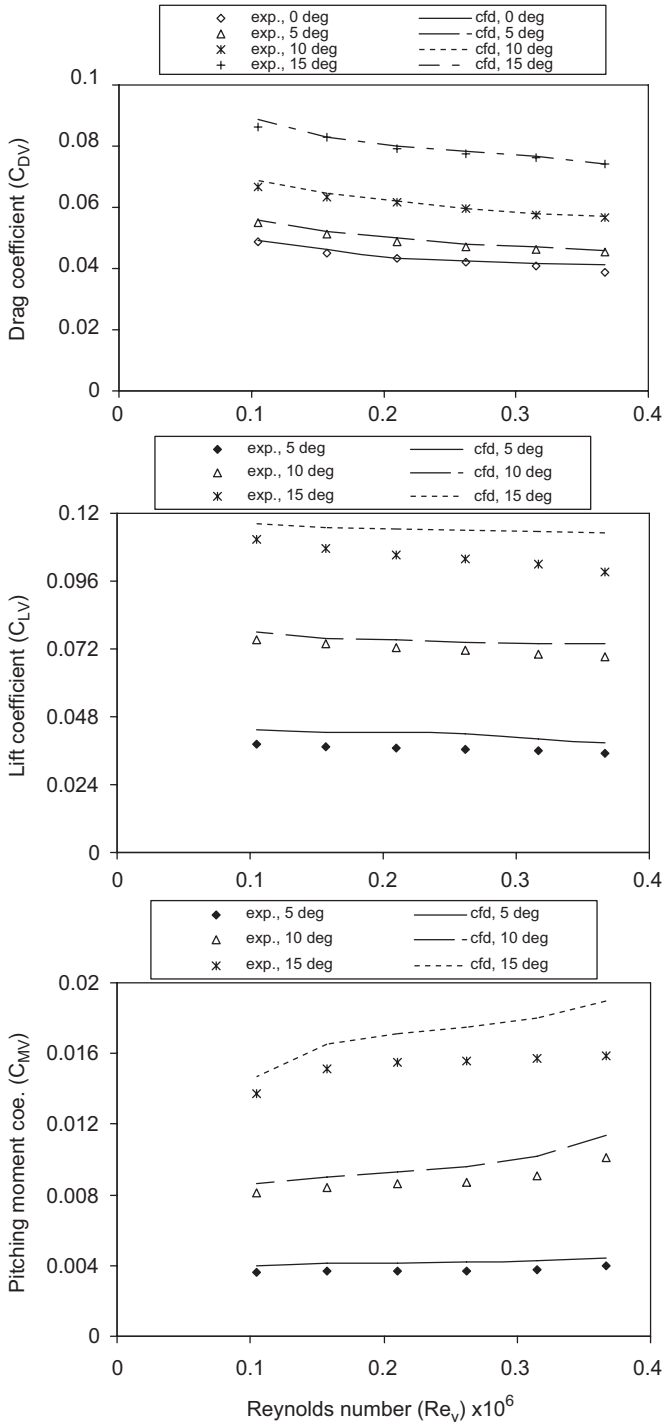

Fig. 6. Influence of Reynolds number (Re_v) on drag, lift and pitching moment coefficient, for various angles of attack.

different angles of attack corresponding to minimum and maximum velocity evincing aforesaid C_{DV} behaviour. The numerical predictions is found to be in good agreement with experimental values with a deviation of 2.57% and 0%, 1.10% and 1.46%, 0.88% and 3.14%, and 0.27% and 3.01% for $\alpha = 0^\circ$, 5°, 10° and 15° corresponding to maximum and minimum velocity. Table 3 provides both measured and numerical drag coefficients along with their percentage deviation for all velocities and angles of attack considered in the current investigation.

Fig. 6 shows a massive increase in lift coefficient, C_{LV} by 97% and 182%, as α increases from 5° to 10° and 15°, for $Re_v = 3.67 \times 10^5$. It is observed from figure as Re_v increases from 1.05×10^5 to 3.67×10^5, C_{LV} value decreases by 8%, 8% and 11%, for $\alpha = 5^\circ$, 10° and 15°, respectively. This can be substantiated by the numerical results (Table 2) by demonstrating appreciable increase in pressure drag coefficient with only a marginal change in friction coefficient, as α increases. Numerical predictions is found to be in good agreement with measured values with minimum and maximum deviation of 4.72% and 12.54%, corresponding to maximum and minimum velocity at $\alpha = 15^\circ$.

Fig. 6 shows the C_{MV} value increases by 152% and 297% as α increases from 5° to 10° and 15° for $Re_v = 3.67 \times 10^5$. In the range of Reynolds number considered, the C_{MV} value increases by 11%, 25% and 16%, for $\alpha = 5^\circ$, 10° and 15°. The centre of pressure changes significantly from 0.082 to 0.11 L (from the nose of model, L = overall length of the model), as α increases from 5° to 15°. It is envisaged that as the longitudinal profile of the body is projected more to the flow, the centre of pressure that would move towards aft attaining a maximum value of about 0.5 L for 90°. The combined effect of increase in angle of attack and the effect of centre of pressure increases C_{MV} at higher pace compared to other hydrodynamic coefficients. Numerical predictions are found to be matching well with measured values with minimum and maximum deviation of 7.29% and 19.05%, corresponding to maximum and minimum velocity at $\alpha = 15^\circ$.

5. Conclusions

The axial, normal, drag, lift and pitching moment coefficients are determined from towing tank experimental study on Afterbody1 for AUV operating conditions for different angles of attack. Results from this study reveals a maximum increase that is observed in normal force coefficient compared to axial force coefficient for the highest speed and angle of attack. Similarly, an increase with descending order of magnitude is observed for pitching moment, lift and drag coefficients, respectively, for highest speed and angle of attack. These results may be useful for design of better guidance and control systems for AUV having similar hull form and operating conditions. A comparison of measured and numerical results shows a good agreement. Hence, for numerical simulation of hydrodynamic force coefficients on AUV hull form resembles Afterbody1, the k-ε AKN turbulence

Table 2
Typical CFD results showing pressure, friction and total drag coefficient for Afterbody1 ($\alpha = 0^\circ$, 5°, 10° and 15°, for $Re_v = 1.05 \times 10^5$ and 3.67×10^5).

Angle of attack (α°)	$Re_v = 1.05 \times 10^5$			$Re_v = 3.67 \times 10^5$		
	Pressure drag coefficient (C_{PV})	Friction drag coefficient (C_{FV})	Drag coefficient (C_{DV})	Pressure drag coefficient (C_{PV})	Friction drag coefficient (C_{FV})	Drag coefficient (C_{DV})
0	0.0022	0.0467	0.0489	0.0103	0.0296	0.0399
5	0.0080	0.0477	0.0557	0.0174	0.0285	0.0459
10	0.0214	0.0475	0.0689	0.0301	0.0269	0.0570
15	0.0431	0.0458	0.0889	0.0520	0.0222	0.0742

Table 3
Comparison of experimental and numerical drag coefficient (C_{DV}), for $\alpha = 0^\circ$, 5°, 10° and 15°.

Volumetric reynolds number, Re_v ($\times 10^5$)	Volumetric drag coefficient (C_{DV})											
	$\propto = 0^\circ$			$\propto = 5^\circ$			$\propto = 10^\circ$			$\propto = 15^\circ$		
	Exp.	CFD	% Dev.	Exp.	CFD	% Dev.	Exp.	CFD	% Dev.	Exp.	CFD	% Dev.
3.67	0.0389	0.0399	2.57	0.0454	0.0459	1.10	0.0565	0.0570	0.88	0.0740	0.0742	0.27
3.15	0.0407	0.0412	1.23	0.0461	0.0469	1.73	0.0574	0.0581	1.22	0.0763	0.0767	0.52
2.62	0.0419	0.0423	0.95	0.0471	0.0480	0.91	0.0594	0.0596	0.34	0.0774	0.0782	1.03
2.10	0.0434	0.0441	1.61	0.0486	0.0500	2.88	0.0617	0.0622	0.81	0.0790	0.0799	1.14
1.57	0.0451	0.0452	0.22	0.0513	0.0519	1.17	0.0634	0.0644	1.58	0.0829	0.0829	0.00
1.05	0.0489	0.0489	0.00	0.0549	0.0557	1.46	0.0668	0.0689	3.14	0.0863	0.0889	3.01

Note: In the above table, Exp. and Dev. stand for experimental and deviation, respectively.

model is found to be suitable from commercial flow solver, ANSYS^{TM} Fluent. Therefore, k-ε AKN turbulence model is quite useful for future hydrodynamic predictions on AUVs operating under various conditions.

Acknowledgement

The first author expresses their gratitude towards the authorities of Indian Institute of Technology Madras, Chennai, for providing necessary facilities.

References

Abe, K., Kondoh, T., Nagano, Y., 1994. A new turbulence model for predicting fluid flow and heat transfer in separating and reattaching flows–1. Flow field calculations. Int. J. Heat and Mass Transfer 37 (1), 139–151.

Ananthakrishnan, P., Zhang, K.-Q., 1998. AUV motion in a wave field. In: Proceedings of the IEEE OCEANS'98 Conference, Nice, France, pp. 1059–1063.

Anil Dash, Panneerselvam, S., Idichandy, V.G., Vendhan, C.P., 1996. Multicomponent force measurement on submerged bodies. In: Proceedings of the International Conference in Ocean Engineering COE'96, IIT Madras, India, 17–20 December, pp. 553–557.

Choi, S.K., Ching, J.C., 1991. Navier–Stokes solution of complete turbulent flow past finite axisymmetric bodies. AIAA Journal 29 (6), 998–1001.

Gertler, M., 1950. Resistance experiments on a systematic series of streamlined bodies of revolution—for application to the design of high-speed submarines. DTRC Report: C-849, Washington, D.C.

Granville, P.S., 1953. The calculation of the viscous drag of bodies of revolution. Naval Department, The David W. Taylor Model Basin, Washington, Report 849.

Hackett, J.E., 2000. Drag, lift and pitching moment increments due to wall constraint in a two-dimensional wind tunnel. In: Proceedings of the Thirty Eighth Aerospace Sciences Meeting and Exhibit, Pers. Communication.

Huang, T.T., Santelli, N., Belt, G., 1978. Stern boundary-layer flow on axisymmetric bodies. In: Proceedings of the Twelfth ONR Symposium on Naval Hydrodynamics. Washington D.C., pp. 127–157.

Jagadeesh, P., Murali, K., 2005. Application of low-*Re* turbulence models for flow simulations past underwater vehicle hull forms. The Journal of Naval Architecture and Marine Engineering 1 (2), 41–54.

Jagadeesh, P., Murali, K., 2006. Investigation of alternative turbulence closure models for axisymmetric underwater hull forms. The Journal of Ocean Technology 1 (2), 37–57.

Mulvany, N., Tu, J.Y., Chen, L., Anderson, B., 2004. Assessment of two-equation turbulence modeling for high Reynolds number hydrofoil flow. International Journal for Numerical Methods in Fluids 45, 275–299.

Nakayama, A., Patel, V.C., 1974. Calculation of the viscous resistance of bodies of revolution. Journal of Hydronautics 8 (4), 154–162.

Patel, V.C., Chen, H.C., 1986. Flow over tail and in wake of axisymmetric bodies: review of the State of the Art1. Journal of Ship Research 30 (3), 202–314.

Patel, V.C., Lee, Y.T., 1977. Thick axisymmetric turbulent boundary layer and near wake of a low-drag body of revolution. Iowa Institute of Hydraulic Research, IIHR Report 210.

Roddy, R.F., 1990. Investigation of the stability and control characteristics of several configurations of the DARPA SUBOFF Model (DTRC Model 5470) from captive-model experiments. David Taylor Research Centre Report DTRC/SHD-1298-08.

Sarkar, T., Sayer, P.G., Fraser, S.M., 1997a. Flow simulation past axisymmetric bodies using four different turbulence models. Journal of Applied Mathematical Modeling 21, 783–792.

Sarkar, T., Sayer, P.G., Fraser, S.M., 1997b. A study of autonomous underwater vehicle hull forms using computational fluid dynamics. International Journal for Numerical Methods in Fluids 25, 1301–1313.

Sayer, P., 1996. Hydrodynamics forces on ROV near the air/sea interface. International journal of offshore and polar engineering 6 (3), 177–183.

Sung, C.H., Griffin, M.J., Tsai, J.F., Huang, T.T., 1993. Incompressible flow computation of forces and moments on bodies of revolution at incidence. I31st Aerospace Sciences Meeting and Exhibit, January 11–14, AIAA 93-0787, pp. 1-10.

Sung, C.H., Fu, T.C., Griffin, M.J., Huang, T.T., 1995. Validation of incompressible flow computation of forces and moments on axisymmetric bodies at incidence. In: Proceedings of the Thirty Third Aerospace Sciences Meeting and Exhibit, January 9–12, AIAA 95-0528, pp. 1–13.

Wilcox, D.C., Rubesin, W.M., 1980 Progress in turbulence modelling for complex flow fields including effects of compressibility. NASA Technical Paper 1517.

Zedan, F.M., Dalton, C., 1979. Viscous drag computation for axisymmetric bodies at high Reynolds numbers. Journal of Hydronautics 13 (2), 52–60.